Construction and Building Materials 191 (2018) 342–353

Contents lists available at ScienceDirect

Construction and Building Materials

journal homepage: www.elsevier.com/locate/conbuildmat

Assessment of coatings for protection of cement paste against microbial induced deterioration through image analysis

Lijuan Kong [a,b,c,*], Jun Fang [a], Xiangming Zhou [c], Mengdi Han [a], Haoran Lu [a]

[a] School of Materials Science and Engineering, Shijiazhuang Tiedao University, Shijiazhuang 050043, China
[b] Hebei Engineering Technology Research Center for Application of High Performance Concrete with Ultra-low Environment Load, Shahe 054100, China
[c] Department of Civil & Environmental Engineering, Brunel University London, Uxbridge, Middlesex UB8 3PH, United Kingdom

HIGHLIGHTS

- Image analysis proved as accurate & labor-saving for studying deterioration of cement paste.
- Uncoated specimen has the most content of S and the least contents of Ca and Si.
- ECTPC has the best resistance to sewage corrosion, followed by CBC and CCCWC.
- Physical barrier effect & bactericidal function protect concrete against sewage attack.
- The image analysis can determine the evolution of deterioration layer.

ARTICLE INFO

Article history:
Received 21 June 2018
Received in revised form 30 September 2018
Accepted 5 October 2018
Available online 10 October 2018

Keywords:
Coating
Cement paste
Microbial induced deterioration
Image analysis
MATLAB

ABSTRACT

In this study, a laboratory method and equipment was developed to accelerate and study the microbial induced deterioration of cementitious materials, and three types of coatings, namely, cement-based capillary crystalline waterproofing coating (CCCWC), cement-based bactericidal coating (CBC) and epoxy coal tar pitch coating (ECTPC) were applied onto the cement paste surface, and their protecting effects were investigated. After immersion in sewage, the microstructure and element distribution of cement paste were characterized by scanning electron microscopy-electron dispersive spectrometry (SEM-EDS). Besides, the distribution of dead/live cells within the biofilm attached to various specimens was examined by confocal scanning laser microscopy (CLSM). To make a quantitative study, the image analysis was adopted. Since both the images obtained belonged to RGB color system, it was found that the image processing program of MATLAB is simple but very helpful for such task. The results indicate that for uncoated specimen, there were the most content of S and the least contents of Ca and Si. However, for coated specimens, the contents of S decreased and that of Ca and Si increased accordingly. ECTPC had the best protective effect on the microbial induced deterioration of concrete, followed by CBC and CCCWC. Besides the physical barrier effect, the bactericidal function of coating has significant contribution for protecting concrete against sewage attack. Furthermore, the image analysis was used to determine the penetration depth of element S in cement paste quantitatively, and based on the change of the S concentration with penetration depth, the surface specimens can be divided into three zones: interior deterioration layer, transition layer and non-corroded layer. The combined use of micro-scale characterization and image analysis can provide a quick, accurate and labor saving method for the deterioration study of coated concrete in sewage environment.

1. Introduction

Concrete has long been used for building the municipal infrastructure due to its excellent durability. However, many wastewater collection and treatment facilities face the problem of concrete deterioration of its structure with time [1]. The mechanism of concrete deterioration suffered from sewage attack is very complex. On top of the physical and chemical effects [2–4], microbial attack is identified as a major source which induce concrete deterioration [5–8], due to the harmful acids produced by the metabolic activity of many bacteria. To protect concrete structures from sewage attack, surface coating is the most widely adopted measure in engineering [9,10]. Generally, the protective coatings of concrete in

* Corresponding author.
E-mail address: klj@stdu.edu.cn (L. Kong).

https://doi.org/10.1016/j.conbuildmat.2018.10.041
0950-0618/

sewage environment can be divided into two categories. One is inert coating, which isolates the concrete from aggressive acidic medium, among them the acid-resistant organic resins are commonly used, such as epoxy resins, polyester resins, urea formaldehyde resins, acrylic resins, polyvinyl chloride, bitumen and so on [11–14]. The other one is active coating, which can protect the base materials through chemical or biological activities. For example, the coating prepared with inorganic or organic cementitious material as the matrix and bactericide as the functional component have exhibited antibacterial or bactericidal capability [15,16].

Diamanti et al. [17] investigated the efficiency of two cementitious coatings modified with acrylic polymers in preventing chloride-induced corrosion by testing the materials permeability to water, water vapour and chlorides. Vipulanandan and Liu [18] reported the performances of two commercially available polyurethane coatings under sulfuric acid environment (representing sewer condition). Muynck et al. [10] and Berndt [19] adopted the accelerated microbiological tests and, through measuring the macro-performance of coated concrete, found that epoxy coating has the best protecting effect. Hewayde et al. [20] used the Sulfate-reducing bacteria (SRB), which were isolated from an anaerobic lab-scale reactor using Desulfovibrio broth, as the medium, and found that coated concrete pipes with either silver oxide or cuprous oxide effectively reduced the SRB count in the nutrient solution. We can see that the effectiveness of surface coatings for protecting concrete from different aggressive medium attack has been studied. However, the protecting effect of different types of coatings in intensified sewage has not been systematically investigated.

In addition, most of the studies focused on the degradation of coatings in aggressive medium. For example, Nazemi and Valix [21] investigated the diffusion and mass transfer of sulphuric acid through epoxy coatings, and in order to validate the predicted result, the penetration depth of acid in coating was measured by sulphur mapping of scanning electron microscopy-electron dispersive spectrometry (SEM-EDS). Buenfeld and Zhang [22] observed the morphology of the polyurethane coated mortar specimens after 3-year exposure to NaCl solution by SEM, and they clearly observed the two-layer structure of the coating with the outer layer being much coarser than the inner layer. Microbial growth inhibition and resistance to biological deterioration of concrete specimens coated with silver-loaded zeolite was also studied by Haile et al. [23], the growth of A. thiooxidans, biological sulfur oxidation, sulfate generation and biomass respiration were tested, as well as the morphology and mineral compositions of concrete specimens. All of the results demonstrated the resistance of silver-loaded zeolite coatings to biological sulfuric acid attack. However, some properties of organic and inorganic coatings are not suitable for comparison against each other. If it was possible to directly study the performance of concrete under coating, it would be more accurate for assessing the protective effect of coating on concrete against sewage attack.

The mechanism of biodegradation and the structure of degraded cement paste specimens were studied using test techniques such as, SEM, X-ray diffraction (XRD) and energy dispersive X-ray analysis (EDXA) [24]. Concrete samples extracted from heavily deteriorated concrete manholes of an Austrian sewer system were analyzed using microbiological, biochemical and mineralogical methods [25]. The results revealed that the elemental accumulation in sample was unequivocally correlated with responding pH levels, associated dissolution and precipitation of solids, as well as with the spatially resolved presence of microbes. Overall, most of the current test methods to assess the performance of coating and concrete are qualitative analysis based. Imaging technique is a good method to characterize the degradation of both concrete and coatings intuitively. It can identify the bugholes [26] and cracks [27] on concrete surface, as well as other forms of chemical attack like alkali silica reaction [28] or chloride attack. Sudbrink et al. [29] and Moradllo et al. [30] used micro X-ray fluorescence (μXRF) to image the presence of silane coatings and chloride in concrete samples. Jensen et al. [31] used electron probe microanalysis (EPMA) to measure chloride concentration profiles in cement paste and concrete samples. In addition, SEM-EDS is also frequently used in characterizing the surface chemistry of the cementitious materials [21]. However, to make a quantitative study, the raw data from images still need to be analyzed by image processing software like toolbox of MATLAB [32,33]. The main functions of MATLAB that can be utilized include original image reading, image information collection, matrix data conversion and characteristic parameters calculation, etc. In summary, the ideal method to investigate the deterioration of coated concrete against sewage attack should be accurate and quick with little work loading and great time saving.

In line with these, in this study, the artificially intensified sewage with high concentration was prepared for the accelerated degradation test, and three different types of coatings were applied on hardened cement paste surface. Then the change in appearance of coating and cement pastes were observed in the sewage corrosion process. The techniques of SEM-EDS and confocal scanning laser microscopy (CLSM) were adopted to characterize the distribution of elements and bacteria in cement paste and the attached biofilm, respectively. Moreover, image analysis was used to quantify the microstructure deterioration of coated and uncoated cement paste specimens. The objective of the present study is to investigate and propose a reliable and labor saving method for deterioration determination and mechanism analysis of coated concrete in sewage environment, which helps in comparing the protective effects among different surface coatings for concrete.

2. Experimental program

2.1. Cement paste specimens

Grade 42.5 Ordinary Portland Cement (Chinese standard GB175-2007) was used in the production of cement paste specimens. The cement paste was prepared with a water/cement ratio of 0.5 and molded in 40 mm × 40 mm × 40 mm cube blocks. After curing (i.e. temperature was kept at 20 °C and the relative humidity was higher than 95%) for 28 days, the cement paste specimens were coated with the three types of coatings, respectively.

2.2. Surface coatings

Three typical protective coatings for cement and concrete were investigated, including cement-based capillary crystalline waterproofing coating (CCCWC), cement-based bactericidal coating (CBC) and epoxy coal tar pitch coating (ECTPC), in this study as shown in Fig. 1. The specific compositions and technology of coatings investigated in this study are summarized in Table 1.

CCCWC has obvious effect on repairing cracks through blocking pores, and can improve the impermeability and corrosion resistance of concrete. CBC has certain bactericidal capability to inhibit the production of biological acid. ECTPC can act as a barrier to isolate the concrete from aggressive acidic medium. Among them, both CCCWC and CBC are cement-based inorganic coatings. Prior to coating, they were mixed with water and stirred for 1 min with an agitator. ECTPC is a type of organic coating. According to the manufacture's guidelines, after mixing the binder with curing agent and cured for 20 min, the diluting agent was added, and then the coating was ready to be used after a secondary mixing. The

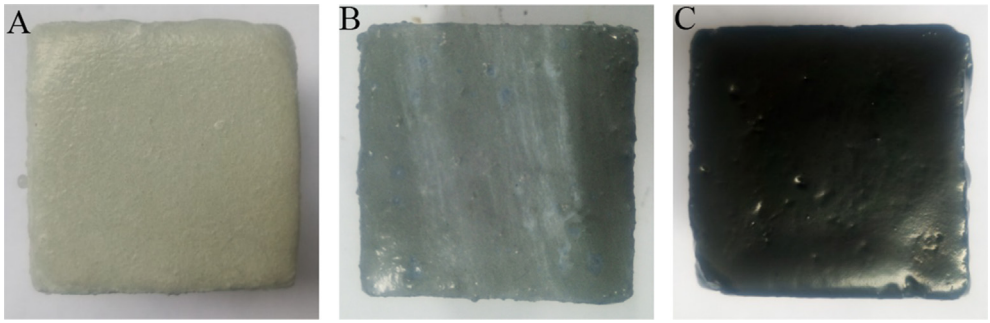

Fig. 1. Cement paste specimens with different coatings: A) CCCWC, B) CBC, C) ECTPC.

Table 1
Compositions and technology of coatings.

Coatings	Mixing ratio	Coating technology	Main components	Functional component
CCCWC	Powder: water = 5:2 (by mass)	2 layers of coats total 4.02 kg/m^2	Ordinary portland cement and refined quartz sand	Special active chemical substances (alkali metal salt, complex compound, etc.)
CBC	Powder: water = 5:2 (by mass)	2 layers of coats total 2.78 kg/m^2	Ordinary portland cement and refined quartz sand	copper phthalocyanine: cuprous oxide: potassium nitrate = 1:1:1
ECTPC	Binder: curing agent = 10:1 (by mass)	4 layers of coats total 2.19 kg/m^2	epoxy resin, coal tar pitch, antirust pigment, auxiliary agent and modified amine	

thickness of all the three types of coating applied on cement paste specimen surface was about 4–6 mm.

2.3. Sewage corrosion test

In order to accelerate the test, the artificially intensified sewage with a chemical oxygen demand (COD) concentration of 6000 mg/L, 20 times the concentration of ordinary sewage, was prepared as follows. First, 1 kg activated sludge, which were obtained from the secondary sedimentation tank in Shijiazhuang Sewage Plant, was used as the parent; then 20 kg nutrient solution, which consisted of starch (200.0 g), glucose (110.0 g), peptone (28.5 g), urea (12.0 g), $(NH_4)_2HPO_4$ (6.7 g), $MgSO_4$ (3.6 g), NaCl (1.2 g), was added into the parent sewage to promote the reproduction of microbes. The in-house sewage corrosion device for concrete, developed for this study, is shown in Fig. 2, which was formed with a plexiglass cylindrical body (400 mm inside diameter, 8 mm thick). An automatic heating rod was fixed to keep the sewage at a constant temperature of 30 °C, which is good for the growth and reproduction of microbes. Moreover, to prevent the sedimentation of sewage and maintain a uniform and stabilized corrosive environment, a mixer was fixed on the center of the device. The uncoated and all sides coated concrete specimens were placed on the shelf and immersed in the sewage, thus the specimens could be corroded fully and evenly as designated. The medium inside the device was replaced with the fresh nutrient solution every 7 days by a pump. The total liquid removed per cycle was less than 30% of the original sewage by volume. The cement paste specimens without and with different coatings were placed into four separate corrosion devices.

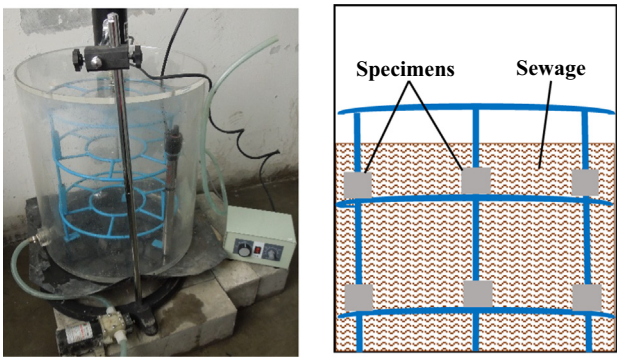

(a) Photo of experiment device (b) Sketch of experiment device

Fig. 2. Sewage corrosion device (a) Photo of experiment device, (b) Sketch of experiment device

2.4. SEM-EDS test procedure

The uncoated and coated cement paste samples (with coating removed) with 10 mm thick were cut from the middle of their exposed surface, and the profile had a length of approximately 20 mm across the surface of each sample. Then the samples was polished by silicon carbide sandpaper of 180 meshes, 600 meshes and 1200 meshes, respectively, until they became as thin as about 5 mm. Ethanol was then used to remove dirt and residue from the polished surface. The penetration depth and relative content of sulphate in artificially intensified sewage can be determined by area mapping of sulphur (S) element through the cross section of samples from outside to inside using SEM-EDS. This was carried out by using Zeiss Gemini SEM 300 with a spectrometer. The parameters of surface scanning were set at the acceleration voltage of 18 KV and resident time of 100 s. Since the maximum range that can be observed by SEM with the lowest magnification factor (i.e. 25 times) is 4.62 mm, the sample was divided into the equal interval segment with a conductive pen to ensure that the dividing line can be observed by SEM, as shown in Fig. 3. Therefore, in this

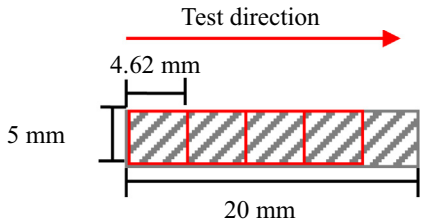

Fig. 3. Illustration of SEM-EDS test for cement paste sample.

study the test range of cement paste samples were 18.48 mm. In addition, the microstructures of different cement paste samples were observed at 3000 magnification, and the distribution of calcium (Ca) and silicon (Si) elements were also examined.

2.5. CLSM test procedure

The viability of bacterial cells in biofilm was determined using the live/dead cell fluorescence staining kit. First, the uncoated and coated cement paste specimens were taken out from sewage, and the biofilm attached to their surface was scraped down and dipped the biofilm in buffer solution, which consist of NaCl (137 mmol/L), KCl (2.7 mmol/L), Na_2HPO_4 (4.3 mmol/L) and KH_2PO_4 (1.4 mmol/L), to rinse off the loose cells. Then, the staining solution was prepared by mixing reagent A and reagent B with the volume ratio of 1:1 and being diluted 200 times with buffer solution. Finally, the microbial cells from the biofilm were stained and incubated for 5 min at 37 °C, subsequently, the samples were observed under Fluoview FV-1000 CLSM. The wavelengths of excitation photon and emission photon were 543 nm and 591 nm, respectively. Under the blue light, the living cells exhibit green while the dead cells red.

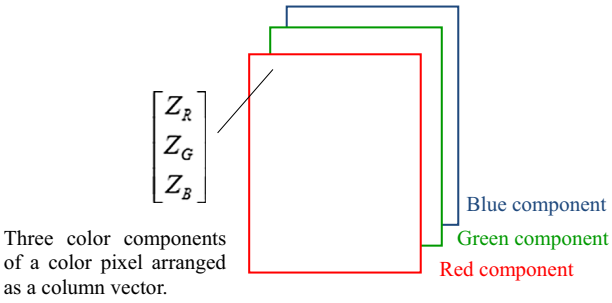

Fig. 4. Schematic illustration of the image pixel in RGB color components [26]. (For interpretation of the references to colour in this figure legend, the reader is referred to the web version of this article.)

2.6. Image analysis technique

The aim of image analysis is to transform a natural form of image into a digital form suitable for computer processing. The pictures obtained by SEM-EDS and CLSM were all color images, so they can be analyzed by the most widely used RGB color system, which is composed of three monochromatic images, known as the red (R), green (G) and blue (B) component images. Each component image corresponds to a two-dimensional function f(x,y) [26]. Therefore, the information of the image can be represented as a digital matrix in the computer, and each element of the matrix has different image characteristic information [34].The schematic diagram of the component pixel in RGB color image is shown in Fig. 4. MATLAB contains extensive image processing tools to extract image information, which can provide simple function calls to achieve that many classic image processing methods like image enhancement, image segmentation and so on can achieve. In this study, the matrix representation method and the operation function of image were used, which can do addition and subtraction linear operations to represent images by using the form of matrix or array. To do this, first, the IMREAD function in MATLAB is used to read the original image, and the information on the image is collected and the images are divided into X row and Y columns according to the pixels that are read in. Then the pictures are converted into matrix data based on that all the color maps are made up of the RGB matrix. Finally the feature of the image is extracted and the related characteristic parameters are calculated.

3. Results and discussion

3.1. Deterioration morphology of uncoated and coated cement paste specimens

3.1.1. Surface morphology

After being immersed in sewage for 1 month, 2 months and 3 months, the surface morphology of various cement paste specimens were observed, respectively, as shown in Fig. 5. The different sets were designated with the following codes: uncoated cement paste specimen (UCS), cement paste coated with CCCWC (CCS),

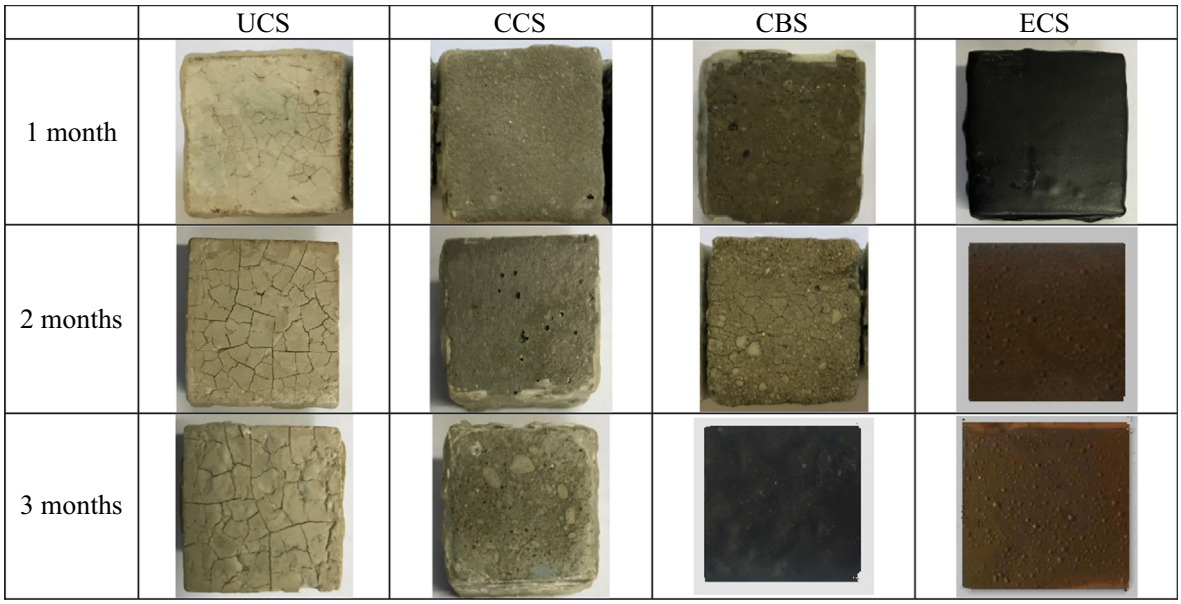

Fig. 5. Surface morphology of cement paste specimens after exposure to sewage.

cement paste coated with CBC (CBS) and cement paste coated with ECTPC (ECS).

It can be seen that after 1 month from the start of sewage degradation experiment, a white and soft layer with many cracks was observed on the surface of UCS, whereas the appearance of other three specimens had little change. With the increase of degradation time, more severe cracks appeared on the surface layer of UCS, which was attributed to the formation of expansive gypsum and ettringite [5,35], and the layer was easily separated from the specimen surface. It is reported that the sulfuric acid, nitric acid and organic acid produced by microbial metabolism, which can react with alkali in the cement, is the main cause of concrete corrosion in sewage [36–38]. For the coated specimens, the color of CCS had no significant change, whereas that of CBS and ECS had changed from grey to black and from black to brown, respectively. Besides, both the inorganic coatings showed signs of spalling and few cracks were observed on the surface of CBS. In comparison, the surface of CCS showed only some voids which is due to the self-healing of CCCWC. The active substance in CCCWC can enter the pores and cracks of concrete with water and react with the ions to form water-insoluble crystals [39,40]. On the other hand, the surface of ECS showed significant amount of air bubbles with loss of gloss and swelling of the top coat.

3.1.2. Section morphology

In addition, the uncoated and coated cement paste specimens were cut and the coatings were stripped off using sand paper, then the cross section morphology of the samples exposed to sewage for different periods was observed, as shown in Fig. 6.

An exterior deterioration layer, which has lighter color and a sharp boundary with the cement matrix, can be seen obviously on the cross-section of all the cement paste specimens except ECS. The surface of UCS had developed a visible exterior deterioration layer after only 1 month immersion in sewage, and with the increase of time, this layer became thicker. In contrast, the exterior deterioration layers of the coated specimens of CCS and CBS were relatively thinner. However, there was no such layer observed for the coated specimen of ECS. For more accurate determination, the thickness of exterior deterioration layer of various cement paste specimens after different immersion periods were calibrated and measured by image-analysis software. The results are listed in Table 2.

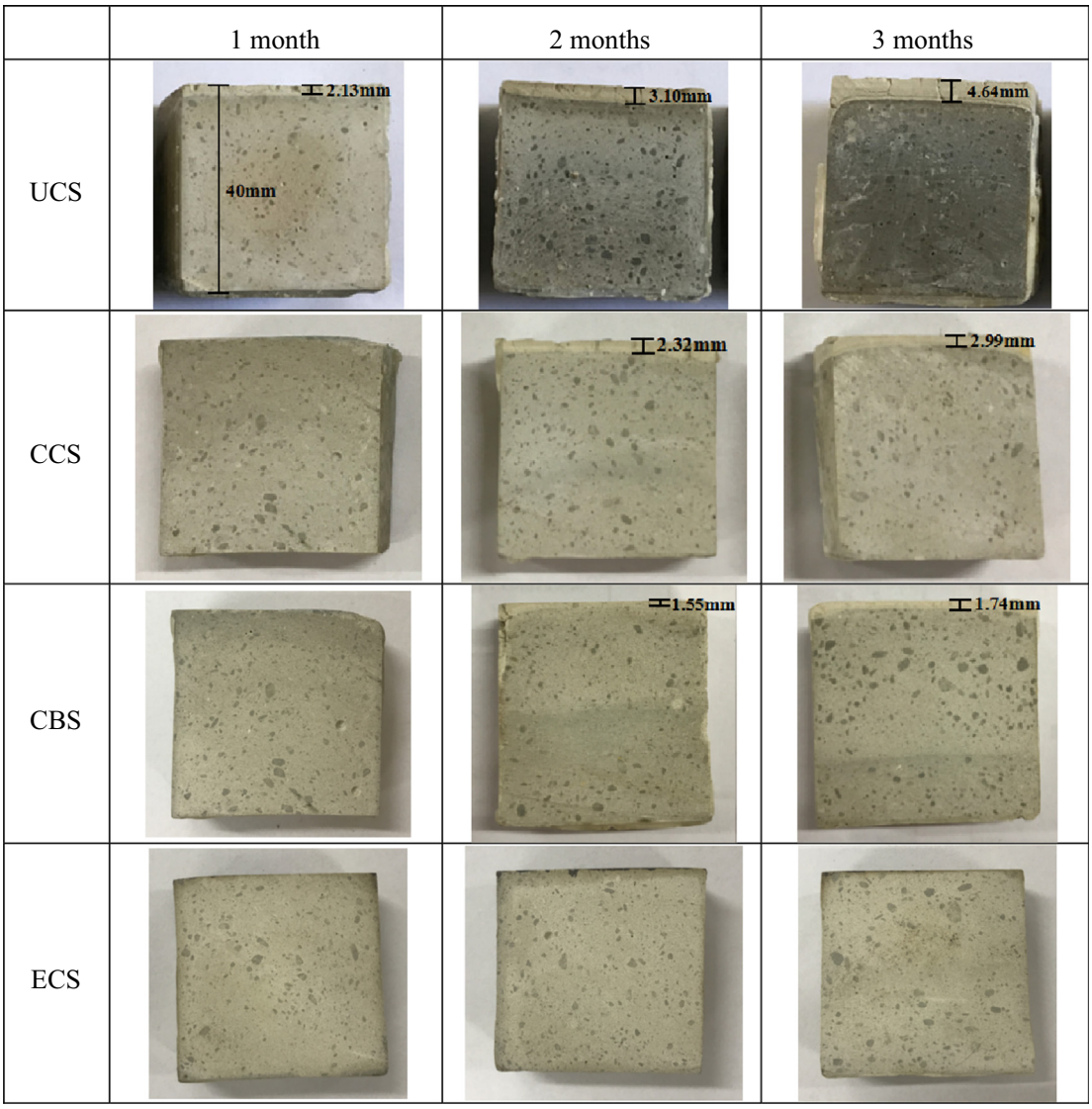

Fig. 6. Section view of cement paste specimens after exposure to sewage.

Table 2
Thickness (mm) of exterior deterioration layer of different specimens.

Specimens	1 month	2 months	3 months
UCS	2.13	3.10	4.64
CCS	0.00	2.32	2.99
CBS	0.00	1.55	1.74
ECS	0.00	0.00	0.00

3.2. Image analysis of cement paste specimens

3.2.1. EDS images

The area scanning image of element S in a specimen surface obtained by EDS is shown in Fig. 7. For each image, an area of 4.62 mm × 2.00 mm was selected to eliminate the interference of other white annotations in the extraction of red pixels. Moreover, the element mappings of S throughout different cement paste specimens were stitched from 4 such images (see Fig. 8).

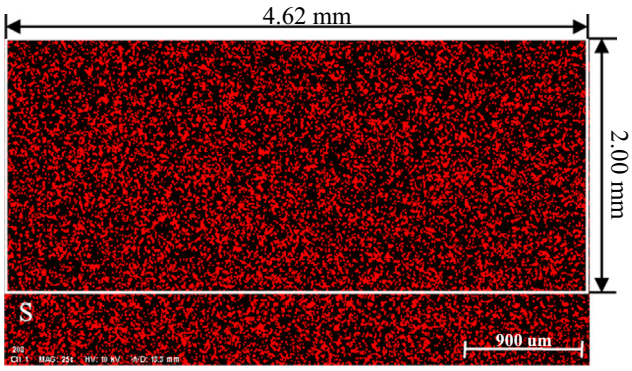

Fig. 7. Area scanning image of element S in cement paste by EDS.

The element distribution within the cement paste specimen was characterized by decreasing S concentration from the surface to the interior. Moreover, the S concentration within UCS increased with time, and after 3 months deterioration it became higher than that within coated specimens, especially for CBS and ECS.

3.2.2. MATLAB programming for image analysis

To make a quantitative comparison of the microstructure deterioration of coated and uncoated cement paste specimens, these EDS images were analyzed by MATLAB. Since the sulphur mapping images only contained black and red pixels, and the red pixel is [x, 0, 0] and black pixel is [0, 0, 0], the image analysis only involves the extraction of red pixels, which can be implemented with the MATLAB codes (see Appendix).

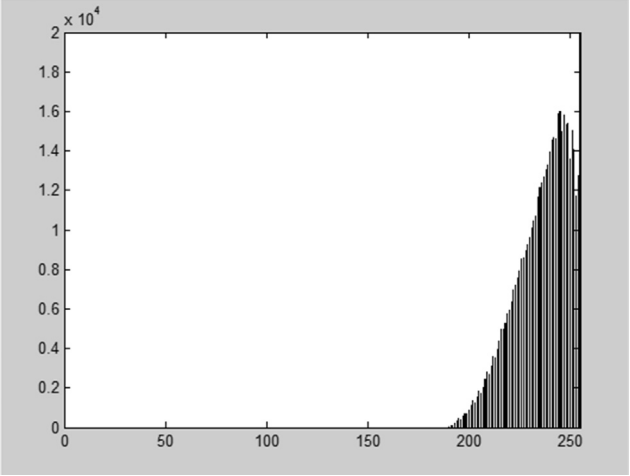

Fig. 9. Histogram of the distribution of image pixels.

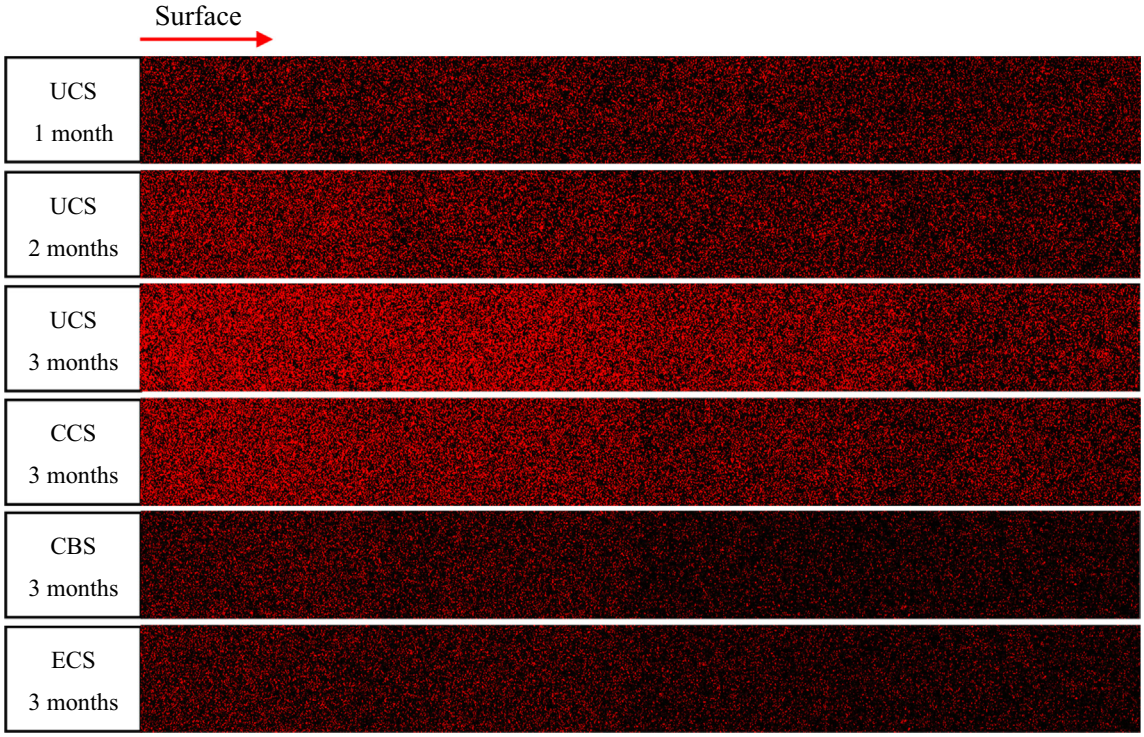

Fig. 8. Sulphur profile map of cement paste specimens.

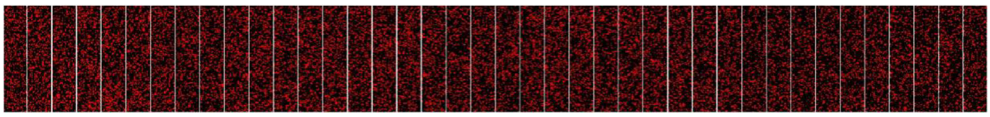

Fig. 10. Interval division of the EDS image.

Take the specimen UCS as an example, the distribution of image pixels after one month exposure to sewage is shown in Fig. 9. It can be seen that when the pixel value was within the range of 200–255, and the proportion of the area of red pixels was close to 91%. For other specimens, the proportions of the area of red pixels were all above 90% within this range. Therefore, the extracted threshold pixel was set to be [200, 255].

Besides, in order to calculate the proportion of red pixels, the image was divided into 2400 columns and 260 rows. For the sake of simplicity, set 60 columns as an interval, and the EDS image can be divided into 40 intervals, as shown in Fig. 10.

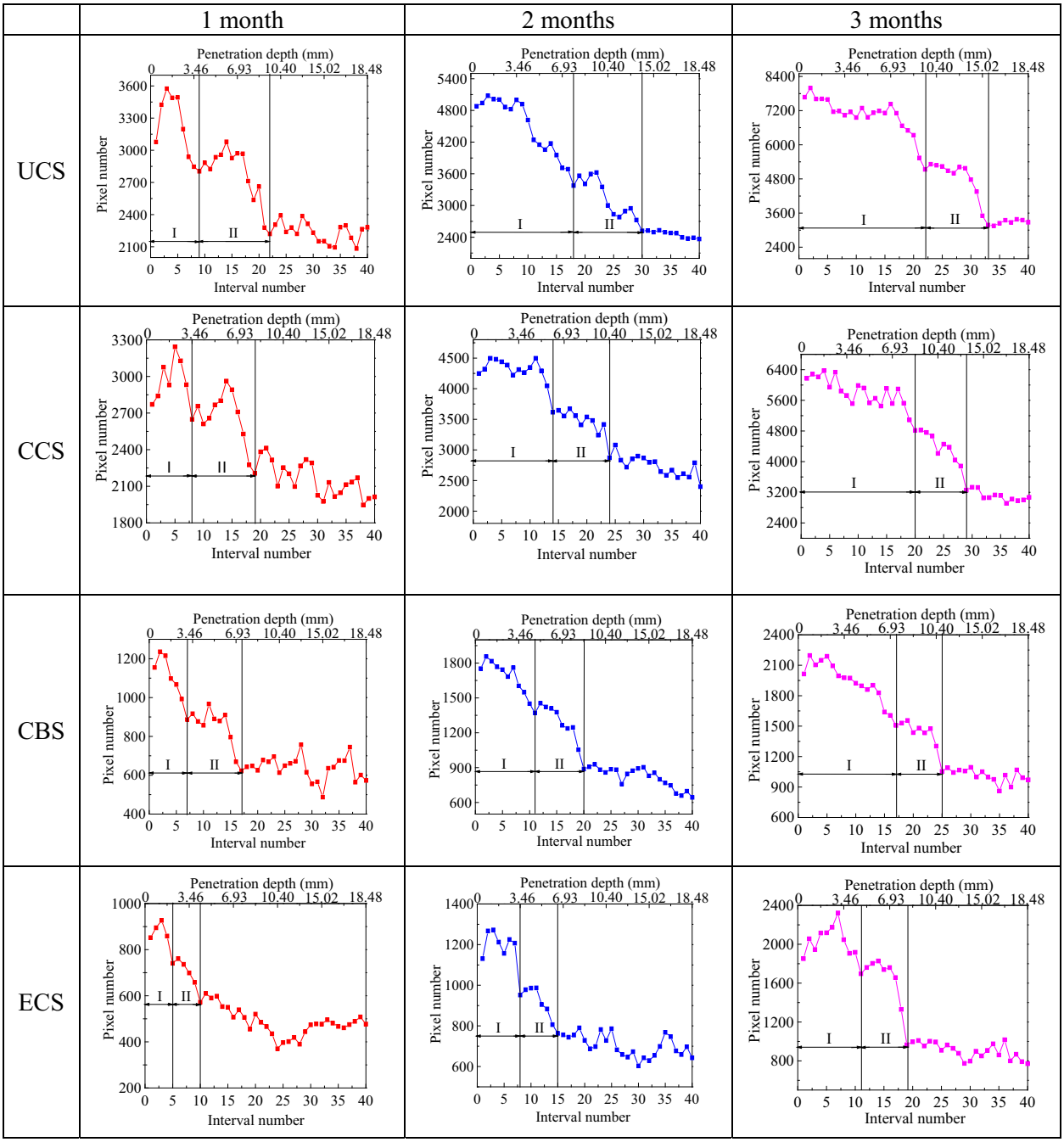

Fig. 11. Penetration depth of sulphur in cement paste specimens.

Table 3
Thicknesses (mm) of zone Ⅰ and zone Ⅱ of different specimens.

Specimen	Zone Ⅰ			Zone Ⅱ		
	1 month	2 months	3 months	1 month	2 months	3 months
UCS	4.16	8.32	10.16	6.01	5.54	5.08
CCS	3.70	6.47	9.24	5.08	4.62	4.16
CBS	3.23	5.08	7.85	4.62	4.16	3.70
ECS	2.31	3.70	5.08	2.31	3.23	3.70

3.2.3. Penetration depth and content of S in specimens

According to the number of red pixels in each interval, the change of the S concentration with penetration depth in specimens can be obtained, as shown in Fig. 11. Obviously, the pixel number of S in all the specimens exhibited a fluctuating and decreasing trend. Furthermore, the test specimens were divided into three zones, which is similar to those identified by other studies [41,42]. Zone I is described as the interior deterioration layer where significant composition and microstructure changes are expected. Zone II is described as a transition layer where moderate changes may occur. The rest of the specimen described as the non-corroded zone which is un-attacked by the sewage. In this study, only the changes in zone I and zone II were analyzed and the thicknesses of interior deterioration layer and transition layer in different specimens are listed in Table 3.

It can be seen that for all the specimens, the thickness of zone I increased gradually with time, whereas that of zone II decreased except ECS. This can be explained as follows. For uncoated and cement based material coated specimens, the deterioration is a damage accumulation process from outside to inside, and with the deterioration of structure of the surface specimens, the cracks and pores formed would result in the penetration of more aggressive medium, so the deterioration rate of zoneⅠwas faster than that of zone II, which led to the increase in thickness of zone I and decrease in thickness of zone II with time. However, for specimen ECS, the organic coating can act as a barrier to prevent sewage penetration, so it suffered the least attack by corrosive media. With the increase of immersion time, some bubbling and swelling appeared on the surface of ECTPC, which resulted in the slow penetration of sewage into a cement paste specimen, so the deterioration of specimen ECS was a gradual development process, and there was simultaneous increase in thickness of zone I and thickness of zone II with time.

Based on the above study, it can be concluded that the exterior and interior deterioration layers, as well as the transition layer, all suffered sewage attack, which can be collectively referred to as the deterioration layer. So the thickness of the deterioration layer is the sum of these three items, and the results are listed in Table 4. It can be seen that the deterioration layer of uncoated specimen was significantly thicker than that of coated specimens. Moreover, these results were plotted with respect to time, as shown in Fig. 12. It can be seen that they all followed a linear relationship of Eq. (1), and the fitting parameters are listed in Table 5. The coefficients of determination (R^2) were all above 0.96, indicating that the fitting results can reflect the change of deterioration layer with time well. The slope of the fit line, which represented the relationship between deterioration layer thickness and time, can be defined as the degradation rate. Taken together, it can be seen that the UCS had both the thickest deterioration layer and the highest degradation rate. Although the deterioration layer of CCS was thinner than that of UCS, their degradation rates were similar. The deterioration layer thickness of ECS was only about one third of that of UCS, and its degradation rate was the lowest.

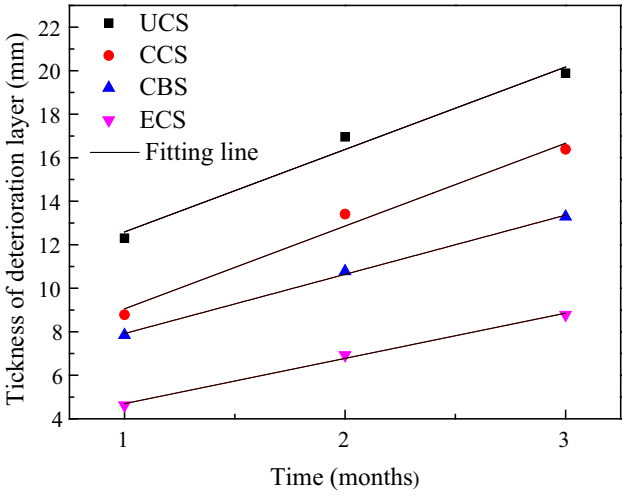

Fig. 12. Linear fitting of the change of deterioration layer thickness with time.

Table 5
Fitting parameters of the change of deterioration layer with time.

Specimen	a	b	R^2
UCS	8.80	3.79	0.96548
CCS	5.25	3.81	0.96914
CBS	5.20	2.72	0.99603
ECS	2.62	2.08	0.99188

$$y = a + bx \quad (1)$$

where x is the corrosion time in month; y is the thickness of deterioration layer in mm; and a and b are the fitting parameters.

In addition, the number of red pixel in the EDS image can represent the content of sulphur element in cement paste specimens. From Fig. 11 it can be seen that the highest pixel number appeared on the position within 3 mm of the specimen surface, and the pixel number corresponding to peak of curve are listed in Table 6. The results show that the content of S element in UCS was significantly higher than that in coated specimens. That is to say, the three

Table 4
Thickness (mm) of the deterioration layer.

Specimen	1 month	2 months	3 months
UCS	12.30	16.96	19.88
CCS	8.78	13.41	16.39
CBS	7.85	10.79	13.29
ECS	4.62	6.93	8.78

Table 6
Maximum pixel number of sulphur in cement paste specimens.

Specimen	1 month	2 months	3 months
UCS	3574	5078	7992
CCS	3243	4496	6373
CBS	1236	1856	2196
ECS	927	1272	2322

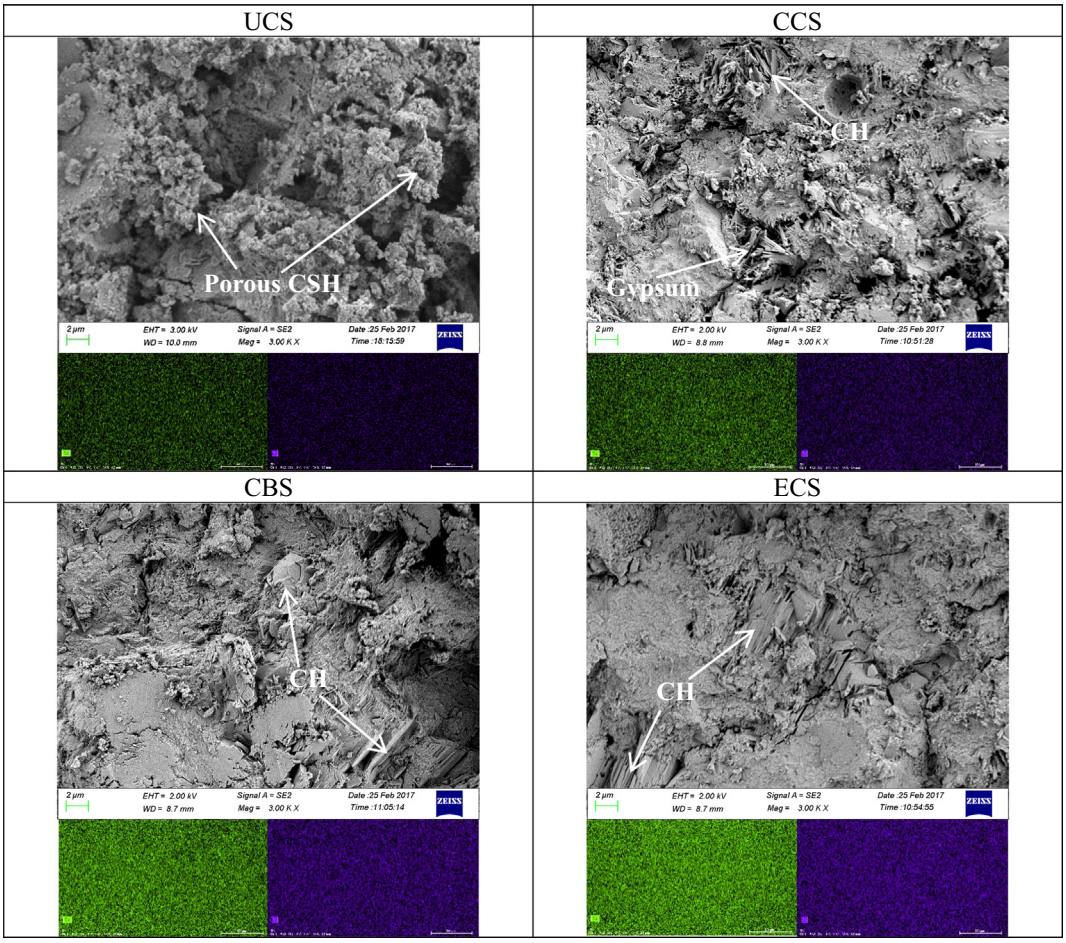

Fig. 13. SEM images and element mappings of Ca (green) and Si (blue) of specimens surface after 2 months exposure to sewage. (For interpretation of the references to color in this figure legend, the reader is referred to the web version of this article.)

coatings all had certain effect of preventing cement paste against sewage attack, especially the organic coating, and the maximum pixel number of ECS was only about one fourth of that of UCS.

3.2.4. SEM observation of specimens

In order to further investigate the deterioration of cement paste specimens, the morphology and composition of uncoated and coated specimens after 2 months exposure to sewage were examined by SEM with the micrographs (taken at the depth of 5 mm from the surface of the specimens) and are shown in Fig. 13, as well the element mappings of Ca (green color) and Si (blue color).

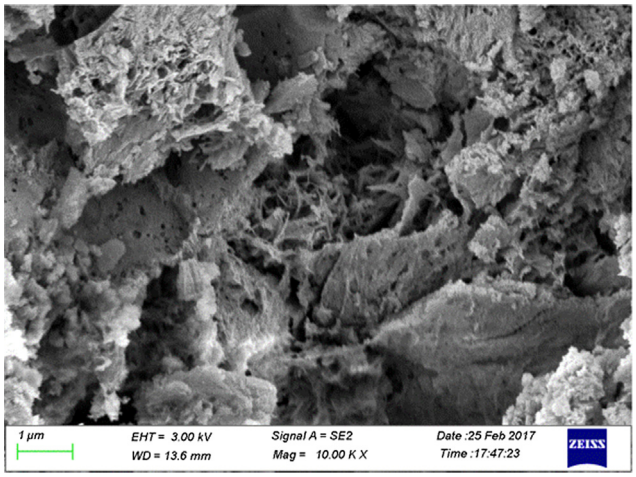

Fig. 14. SEM image of porous CSH.

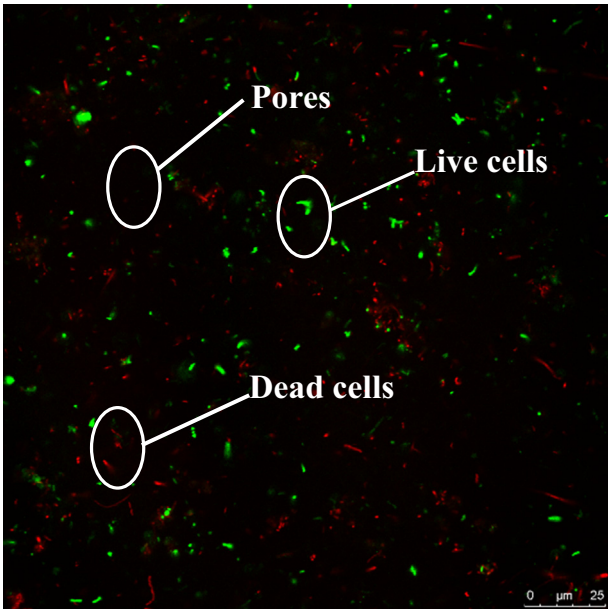

Fig. 15. CLSM image of biofilm.

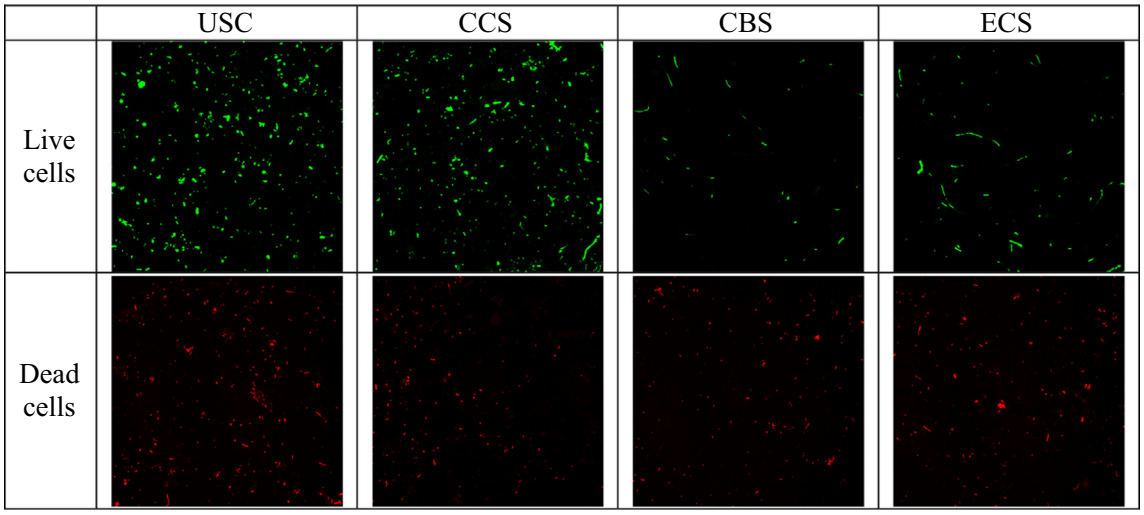

Fig. 16. Distribution of live and dead cells within the biofilm attached to different specimens.

It can be seen that the microstructure of UCS becomes loose, and calcium hydroxide (CH) crystal could barely be found. Moreover the hydrated calcium silicate (CSH) gels became very porous, hence lost it binding capacity (see Fig. 14). In the micrograph of CCS, the cement paste structure became denser with less CH crystal, and some short needle shaped gypsum crystals were observed in the pores. In specimens CBS and ECS, some flattened CH crystals and cluster like CSH gels could be observed. Such closely packed products led to the formation of a relative dense structure, particularly in the case of ECS. Obviously, the deterioration of concrete microstructure had been prevented by surface coatings in varying degree. From the area scanning images of elements Ca and Si on each specimen surface, it can be seen that both the green and blue colors of the element mappings of ECS were the brightest, followed by that of CBS, CCS and UCS, indicating that the Ca and Si contents of ECS were the highest, whereas that of UCS were the lowest. As it is well known, the CH and CSH are the main products of cement hydration, so the decrease of the contents of Ca and Si in cement paste indicated the dissolution and consumption of hydrates due to the sewage attack. This is consistent with the results obtained in S analysis.

3.3. Image analysis of biofilm

After being immersed in sewage for one month, the bacterial colonies slowly gathered and finally formed a complete and mature biofilm on the surface of uncoated and coated specimens. The CLSM image is shown in Fig. 15. Under the blue light, the live cells exhibit green, the dead cells exhibit red while the pores black. To further compare the distribution of dead/live cells within the biofilm attached to different specimens, the images of live cells and dead cells were separated (see Fig. 16) and analyzed by MATLAB, respectively. The extracted threshold pixel was set to be [100, 255] by observing the histogram of the distribution of image pixels. The MATLAB code implementation process is similar to that for EDS image analysis.

Table 7
Area fraction of live/dead cells within the biofilm attached to different specimens (%).

	UCS	CCS	CBS	ECS
Live cells	2.31	2.19	0.22	0.49
Dead cells	0.87	0.40	0.44	0.52

Based on the image analysis, the area fraction of live and dead cells within the biofilm attached to different specimens can be calculated with the results presented in Table 7. By contrast, it can be found that both the numbers of live cells within the biofilms attached to UCS and CCS were higher, whereas that within the biofilms attached to CBS and ECS had a sharp decrease, especially for CBS. This is mainly due to the copper phthalocyanine and cuprous oxide that was contained in CBC, which can combine with the enzymes that required for microbes metabolism, thereby killing or inhibiting their reproduction [43]. Moreover, the coal tar pitch in ECTPC also had certain level of toxicity that can destroy the microbial cell structure, and the epoxy resin can resist biological attack to a certain degree [44]. It is worth noting that although the area fraction of live cells with the biofilm attached to CBS and ECS decreased greatly, the area fraction of dead cells with them had no remarkable increase, even becoming lower than that of dead cells with the biofilm attached to UCS. This may be due to the falling-off of some dead microbes. The reduction of live cells fraction can decrease the production of extracellular polymeric substances (EPS), which is very important in promoting the microbe aggregation and structure stability.

4. Conclusions

1. In order to propose a direct and accurate method for deterioration determination of coated concrete in sewage environment, the image analysis technique was adopted to quantitatively analyze the microbial resistance of different coatings, which is very important to the anti-sewage attack of concrete. Both the images obtained by SEM-EDS and CLSM belong to RGB color system, so the extraction of image feature was only focused on the color, and the image processing program of MATLAB can be readily used for such task.
2. The elemental distribution in specimens can reflect the deterioration of cement paste well. For uncoated specimen, there were higher content of S and less content of Ca and Si. However, for coated specimens, the contents of S decreased and that of Ca and Si increased accordingly. Among them, the ECTPC had the best protection effect on the microbial induced deterioration of concrete, which can be attributed to both the barrier and antibacterial effects, followed by CBC and CCCWC. This suggests that the bactericidal effect of CBC was much better than the crack self-repairing of CCCWC on protecting concrete against sewage attack.

3. In this study, the image analysis was used to determine the penetration depth of element S in cement paste quantitatively. Furthermore, based on the change of the S concentration with penetration depth, the surface specimens can be divided into three zones: interior deterioration layer, transition layer and non-corroded layer. The combined use of micro-scale characterization and image analysis can provide a quick and reliable method for the study of concrete deterioration.

Conflict of interest

None.

Acknowledgements

This work was financially supported by the National Nature Science Foundations of China (51878421), Outstanding Young People of University Science and Technology Research of Hebei Province (BJ2016049) and Hebei Key Discipline Construction Project. The first author would like to thank China Scholarship Council (201708130034) for sponsoring her one-year visit to Brunel University London during which this paper was completed.

Appendix

The MATLAB script for EDS images analysis is as follows:

```
d1 = D (:, :, 1); Red
d2 = D (:, :, 2); Green
d3 = D (:, :, 3); Blue
EK = [ ];
EK = [ ];
for i = 1 : length (d1 (1, :))
  n=0;
  for k = 1 : length (d1 (:, 1))
    if d1(k, i) >= 200&d1 (k, i) <= 255%
      n = n+1;
    else
      n = n;
    end
  end
  EK = [EK, n];
End
m = 60; % The interval width.
MM = [ ];
for j = 1 : length (EK) / m
  s = sum (EK ((j-1) * m + 1 : (j-1) * m + m)); % The total number
   of red pixels extracted from a single interval
  MM = [MM, s] % The total number of red pixels in each
   interval
  nn = MM / (length (d1 (:, 1)) * m) % The proportion of red
   pixels in each interval
End
```

References

[1] M. O'Connell, C. Mcnally, M.G. Richardson, Biochemical attack on concrete in wastewater applications: a state of the art review, Cem. Concr. Compos. 32 (2010) 479–485.
[2] J.Y. Han, Z.H. Gao, X.W. Zhang, Non-uniform damage of primary sedimentation pool concrete by city sewage, China J. Civil Eng. 38 (2005) 45–49.
[3] G. Jiang, E. Wightman, The role of iron in sulfide induced corrosion of sewer concrete, Water Res. 49 (2014) 166–174.
[4] H. Yuan, P. Dangla, P. Chatellier, T. Chaussadent, Degradation modelling of concrete submitted to sulfuric acid attack, Cem. Concr. Res. 53 (2013) 267–277.
[5] T. Mori, T. Nonaka, K. Tazaki, Interaction of nutrients, moisture and pH on microbial corrosion of concrete sewer pipes, Water Res. 26 (1992) 29–37.
[6] E. Vinck, A. Beeldens, Chemical, microbiological, and in situ test methods for biogenic sulfuric acid corrosion of concrete, Cem. Concr. Res. 30 (2000) 623–634.
[7] D. Nica, J.L. Davis, L. Kirby, Isolation and characterization of microorganisms involved in the biodeterioration of concrete in sewers, Int. Biodeter. Biodegr. 46 (2000) 61–68.
[8] S. Valls, A. Yagüe, E. Vázquez, Physical and mechanical properties of concrete with added dry sludge from a sewage treatment plant, Cem. Concr. Res. 34 (2004) 2203–2208.
[9] M. Fiertak, E. Stanaszek-Tomal, Biological corrosion of polymer-modified cement bound materials exposed to activated sludge in sewage treatment plants, Procedia Eng. 65 (2013) 335–340.
[10] W.D. Muynck, N.D. Belle, W. Verstraete, Effectiveness of admixtures, surface treatments and antimicrobial compounds against biogenic sulfuric acid corrosion of concrete, Cem. Concr. Compos. 31 (2009) 163–170.
[11] S.D. Jagtap, S.P. Tambe, R.N. Choudhari, B.P. Mallik, Mechanical and anticorrosive properties of non toxic coal-tar epoxy alternative coating, Prog. Org. Coat. 77 (2014) 395–402.
[12] C. Valentini, J. Fiora, G. Ybarra, A comparison between electrochemical noise and electrochemical impedance measurements performed on a coal tar epoxy coated steel in 3% NaCl, Prog. Org. Coat. 73 (2012) 173–177.
[13] M.D. Nguyen, J.W. Bang, A.S. Bin, S.R. Kim, Y. Kim, K.H. Hwang, V.H. Pham, W.T. Kwon, Novel polymer-derived ceramic environmental barrier coating system for carbon steel in oxidizing environments, J. Eur. Ceram Soc. 37 (2017) 2001–2010.
[14] A. Husain, O. Al-Shamah, A. Abduljaleel, Investigation of marine environmental related deterioration of coal tar epoxy paint on tubular steel pilings, Desalination 166 (2004) 295–304.
[15] R. Wang, K.G. Neoh, E.T. Kang, Integration of antifouling and bactericidal moieties for optimizing the efficacy of antibacterial coatings, J. Colloids Interface Sci. 438 (2015) 138–148.
[16] G. Xiao, X. Zhang, Y. Zhao, H. Su, T. Tan, The behavior of active bactericidal and antifungal coating under visible light irradiation, Appl. Surf. Sci. 292 (2014) 756–763.
[17] M.V. Diamanti, A. Brenna, F. Bolzoni, M. Berra, T. Pastore, M. Ormellese, Effect of polymer modified cementitious coatings on water and chloride permeability in concrete, Constr. Build. Mater. 49 (2013) 720–728.
[18] C. Vipulanandan, J. Liu, Glass-fiber mat-reinforced epoxy coating for concrete in sulfuric acid environment, Cem. Concr. Res. 32 (2002) 205–210.
[19] M.L. Berndt, Evaluation of coatings, mortars and mix design for protection of concrete against sulphur oxidising bacteria, Constr. Build. Mater. 25 (2011) 3893–3902.
[20] E. Hewayde, G. Nakhla, E. Allouche, P. Mohan, Beneficial impact of coatings on biological generation of sulfide in concrete sewer pipes, Struct. Infrastruct. Eng. 3 (2007) 267–277.
[21] M.K. Nazemi, M. Valix, Evaluation of acid diffusion behaviour of amine-cured epoxy coatings by accelerated permeation testing method and prediction of their service life, Prog. Org. Coat. 97 (2016) 307–312.
[22] N.R. Buenfeld, J.Z. Zhang, Impedance spectroscopy monitoring of a polyurethane coating on mortar exposed to NaCl solution, J. Mater. Sci. 35 (2000) 39–44.
[23] T. Haile, G. Nakhla, E. Allouche, S. Vaidya, Evaluation of the bactericidal characteristics of nano-copper oxide or functionalized zeolite coating for bio-corrosion control in concrete sewer pipes, Corros. Sci. 52 (2010) 45–53.
[24] A. Yousefi, A. Allahverdi, P. Hejazi, Accelerated biodegradation of cured cement paste by Thiobacillus species under simulation condition, Int. Biodeter. Biodegr. 86 (2014) 317–326.
[25] C. Grengg, F. Mittermayr, G. Koraimann, F. Konrad, M. Szabó, A. Demenyd, M. Dietzel, The decisive role of acidophilic bacteria in concrete sewer networks: a new model for fast progressing microbial concrete corrosion, Cem. Concr. Res. 101 (2017) 93–101.
[26] B. Liu, T. Yang, Image analysis for detection of bugholes on concrete surface, Constr. Build. Mater. 137 (2017) 432–440.
[27] A. Mazzoli, S. Monosi, E.S. Plescia, Evaluation of the early-age-shrinkage of fiber reinforced concrete (FRC) using image analysis methods, Constr. Build. Mater. 101 (2015) 596–601.
[28] N. Castro, B.J. Wigum, Assessment of the potential alkali-reactivity of aggregates for concrete by image analysis petrography, Cem. Concr. Res. 42 (2012) 1635–1644.
[29] B. Sudbrink, M.K. Moradllo, Q. Hu, M.T. Ley, J.M. Davis, N. Materer, A. Apblett, Imaging the presence of silane coatings in concrete with micro X-ray fluorescence, Cem. Concr. Res. 92 (2017) 121–127.
[30] M.K. Moradllo, B. Sudbrink, Q. Hu, M. Aboustait, B. Tabb, M.T. Ley, J.M. Davis, Using micro X-ray fluorescence to image chloride profiles in concrete, Cem. Concr. Res. 92 (2017) 128–141.
[31] O.M. Jensen, A.M. Coats, F.P. Glasser, Chloride ingress profiles measured by electron probe micro analysis, Cem. Concr. Res. 26 (1996) 1695–1705.
[32] X. Zhu, S. Ai, D. Fang, B. Liu, X. Lu, A novel modeling approach of aluminum foam based on MATLAB image processing, Comp. Mater. Sci. 82 (2014) 451–456.
[33] W. Deng, W. Ding, H. Zhang, Application of MATLAB in figure image processing and analysis, J. Agric. Mech. 6 (2006) 194–198.
[34] B.Q. Chen, H.L. Liu, F.B. Meng, Current situation and development direction of digital image processing technology, J. Jishou Univ. Nat. Sci. Ed. 30 (2009) 63–71.

[35] L. Kong, B. Zhang, J. Fang, Effect of bactericide on the deterioration of concrete against sewage, J. Mater. Civ. Eng. 30 (2008) 1–12.
[36] A. Attal, M. Brigodiot, P. Camacho, J. Manem, Biological mechanisms of H_2S formation in sewer pipes, Water Sci. Technol. 26 (1992) 907–914.
[37] K.S. Cho, T. Mori, A newly isolated fungus participates in the corrosion of concrete sewer pipes, Water Sci. Technol. 31 (1995) 263–271.
[38] J.D. Gu, T.E. Ford, N.S. Berke, R. Mitchell, Biodeterioration of concrete by fungus Fusarium, Int. Biodeter. Biodegr. 41 (1998) 101–109.
[39] J.Y. Yu, W.L. Li, D.X. Guo, Study on crack self-healing performance of concrete with CCCWC, China Build. Waterproof 8 (2009) 14–16.
[40] Y.C. Kuang, J.P. Ou, Experiment and research on permeable crystallization self–repairing performance of concrete, J. Rail. Sci. Eng. 5 (2008) 6–10.
[41] A. Bertron, J. Duchesne, G. Escadeillas, Accelerated tests of hardened cement pastes alteration by organic acids: analysis of the pH effect, Cem. Concr. Res. 35 (2005) 155–166.
[42] C. Grengg, F. Mittermayr, G. Koraimann, The decisive role of acidophilic bacteria in concrete sewer networks: a new model for fast progressing microbial concrete corrosion, Cem. Concr. Res. 101 (2017) 93–101.
[43] H.F. Liu, L. Huang, T. Liu, H.U. Yulong, Application and progress in bactericide of sulfate reducing bacteria, J. Chin. Soc. Corros. Protect. 29 (2009) 154–160.
[44] H.Y. Sun, Z.N. Li, S.G. Chen, Development of EA anti-microbial paint, Mod. Paint Finish 4 (2002) 1–3.